Deformation Signals at Mud Volcano in Kambing Island Detected by L-band InSAR

Naufal Setiawan*[1)], Masato Furuya[2)]
[1)] Geomatic Engineering, Faculty of Mineral Technology, Universitas Pembangunan Nasional "Veteran" Yogyakarta, Indonesia.
[2)] Department of Earth and Planetary Sciences, Faculty of Science, Hokkaido University, Sapporo, Japan.
* Corresponding author: naufal.setiawan@upnyk.ac.id

Abstract – Mud volcanoes are generated by fluid and solid material extrusion from their mud reservoir and are predominantly found at convergent plate margins. Kambing Island is a small island in Eastern Timor, Indonesia, where the Australian continental plate collides with the Banda Sea plate. The previous geological study identified active mud volcano on this island, but it is still unclear whether and to what extent they are active. In this work, we attempt to detect surface deformation due to the mud volcanoes activism in Kambing island using the Advanced Land Observing Satellite/ Phased Array Type L-band Synthetic Aperture Radar (ALOS/PALSAR) Interferometry Synthetic Aperture Radar (InSAR). The ALOS/PALSAR datasets consist of 12 ascending and 5 descending Synthetic Aperture Radar (SAR) data from 2006 to 2011. Although the results indicate surface deformation signals are hardly detected in the interferogram pairs due to lost coherence and atmospheric noise, we could highlight the episodic occurrence of surface deformation signals between April and November 2008 reaches 6.4 cm moving away from the satellite line of sight. In the future, to back up our findings, further field surveys or long-term InSAR are needed.

***Keywords**:* mud volcano, InSAR, deformation.

INTRODUCTION

Mud volcanoes are associated with the extrusion process of fluid mixed with solid material from its source layer (mud reservoir). Multiple mechanisms are necessary for the formation of mud volcanoes, including structural association due to tectonic earthquake activity, sediment over-pressuring and accompanying fluid emission, density inversion (Kopf, 2002). The last is considered a primary prerequisite for sediment from the mud reservoir to ascend (Kopf, 2002; Dimitrov, L. I, 2002). The feature of mud volcanoes defines as (1) domes shaped, which the most elevated point being the conduit, (2) the others may be relatively flat, for example, mud basin with depressions (Kopf, 2002). Furthermore, the size of mud volcanoes may vary depending on the outflowing mud frequency and its viscosity (Dimitrov, L. I, 2002). Mud volcanoes with colossal size and everlasting geological structures are morphologically similar to a magmatic volcanoes. The distribution of mud volcanoes around the world is immense, both offshore and onshore, predominantly occurred at convergent plate margins (Milkov, A, 2000). In the context of onshore mud volcanoes, the area expanding from the Mediterranean Sea to the Tethyan belt is the place where most mud extrusion is known to date (including Azerbaijan, south Greece, Iran, and Turkmenistan).

Our research area is Kambing Island, located in Eastern Timor, Indonesia. In the southern part of Eastern Timor, the northern margin of the Australian continental plate meets the Banda Sea plate (Figure 1). Previous geologic maps derived from the interpretation of aerial photographs identified active mud volcanoes in Kambing Island (Barber et al., 1986).

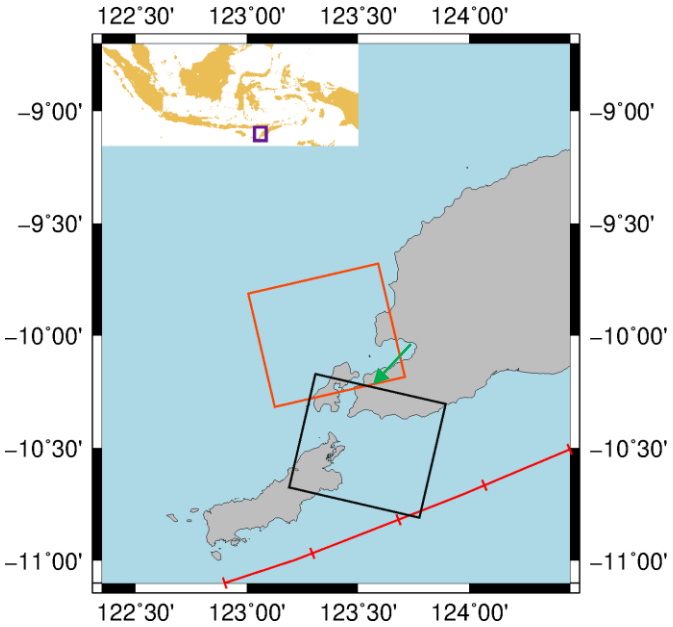

Figure 1. Research study area, Kambing Island (indicated by green arrow). Ascending path (frame 6980) showed by the orange rectangle. While descending path (frame 3830), as shown by the black rectangle. Redline indicates the fault line; the Australian continental plate collides with the Banda Sea plate.

Synthetic Aperture Radar (SAR) uses coherent radar and Doppler beam sharpening to overcome the limitation of Real Aperture Radar (RAR) in terms of low azimuth resolution (R. F. Hanssen, 2002; Moreira et al., 2013). The invention of SAR was coined by Carl Wiley in 1951. The first SAR satellite launched in space was Seasat in 1978. Since the first SAR satellite mission, a lot of follow-on SAR missions operated by different institutions. Some of the examples are Sentinel-1 (European Space Agency), ALOS-2 (Japan Aerospace Agency), Radarsat (Canadian Space Agency), TerraSAR-X (German Aerospace Center), and so on. SAR's unique imaging capability observes the earth independent from the availability of the sun and cloud coverage.

The Single Look Complex Image (SLC) of SAR consist of amplitude and phase value. The amplitude of SLC in a single SAR acquisition is usable after reducing the speckle noise (multi-looking). Meanwhile, the phase image in a single SAR acquisition is impractical because it is impossible to interpret the physical meaning (Furuya, M, 2011). Interferometric Synthetic Aperture Radar (InSAR) exploits the range difference between the two-phase in the same path and frame of SAR acquisition. This is denoted as two-way travel time;

$$\Delta\emptyset = \frac{4\pi}{\lambda}(r1 - r2) \quad (1)$$

where λ is the wavelength, r1 is the range in the first SAR acquisition, r2 is the range in the second SAR acquisitions, and $\Delta\emptyset$ is the phase difference. InSAR is useful for studying various geophysical phenomena, for instance: earthquakes (Hussain et al., 2016) and deformation induced by mud volcanoes (Antonielli et al., 2014; Fukushima et al., 2009; Iio & Furuya, 2018). In this study, we use L-band InSAR to detect surface deformation related to mud volcano activity on Kambing Island.

METHODS

We use L-band Synthetic Aperture Radar (SAR) with a wavelength of 23.6 cm. The advantage of the L-band compared to shorter wavelength can penetrate over dense vegetation and maintain coherence (Funning & Garcia, 2019). We collected the images of Advanced Land Observing Satellite/ Phase Array type L-band Synthetic Aperture Radar (ALOS/PALSAR) from 2006 to 2011. Figure 1 shows the observation scene of ALOS/PALSAR. Details on ALOS/PALSAR data are listed in Table 1 and Table 2. We cropped the ocean areas and adjacent islands (Semau island) to speed up processing time.

Table 1. ALOS/PALSAR ascending datasets.

Observation date	Path	Frame	Off-nadir angle	Scene_Id
20061229	408	6980	34.3	ALPSRP049526980
20070213	408	6980	34.3	ALPSRP056236980
20080101	408	6980	34.3	ALPSRP103206980
20080216	408	6980	34.3	ALPSRP109916980
20080402	408	6980	34.3	ALPSRP116626980
20081118	408	6980	34.3	ALPSRP150176980
20090103	408	6980	34.3	ALPSRP156886980
20090218	408	6980	34.3	ALPSRP163596980
20091121	408	6980	34.3	ALPSRP203856980
20100106	408	6980	34.3	ALPSRP210566980
20100221	408	6980	34.3	ALPSRP217276980
20110109	408	6980	34.3	ALPSRP264246980

Table 2. ALOS/PALSAR descending datasets.

Observation date	Path	Frame	Off-nadir angle	Scene_Id
20081122	70	3830	34.3	ALPSRP150683830
20100412	70	3830	34.3	ALPSRP224493830
20100528	70	3830	34.3	ALPSRP231203830
20101128	70	3830	34.3	ALPSRP258043830
20110113	70	3830	34.3	ALPSRP264753830

We utilize GAMMA software (licensed to Space Geodesy laboratory, Hokkaido University) to create interferograms. Assuming higher coherence of the interferogram is achievable by maintaining the temporal separation as short as possible, the slave data become the subsequent master data in the next interferogram pair creation (Iio & Furuya, 2018). Details on the interferogram pair are listed in Table 3 for ascending and Table 4 for descending pairs, respectively. We remove the topographic fringe in the interferogram using the ALOS World 3D-30m (AW3D30) Digital Elevation Model (DEM) data. The spatial resolution of the AW3D30 is one arc second, ~30 m × 30 m resolution. During the processing step, the original range and azimuth pixel spacing were multi-looked by factors 2 and 6, respectively. We applied adaptive spectral filtering (Goldstein & Werner, 1998) with 0.5 of the exponent for non-linear filtering. In the phase unwrapping procedure, we apply a minimum cost flow algorithm (Costantini, 1998). We eliminate the long-wavelength phase trends in the interferogram by using low-order polynomial.

Table 3. Interferogram pairs from ascending data.

Pair no.	Date	Temporal (days)	Perpendicular Baseline (m)
1	20061229-20070213	46	1214
2	20070213-20080101	322	-1068
3	20080101-20080216	46	477
4	20080216-20080402	46	-329

5	20080402-20081118	230	1565
6	20081118-20090103	46	-274
7	20090103-20090218	46	-109
8	20090218-20091121	276	-414
9	20091121-20100106	46	-335
10	20100106-20100221	46	100
11	20100221-20110109	322	-997

Table 4. Interferogram pairs from descending data.

Pair no.	Date	Temporal (days)	Perpendicular Baseline (m)
1	20081122-20100412	506	-1104
2	20100412-20100528	46	58
3	20100528-20101128	230	-184
4	20101128-20110113	46	-205

RESULT AND DISCUSSION

Interferogram result from ascending data

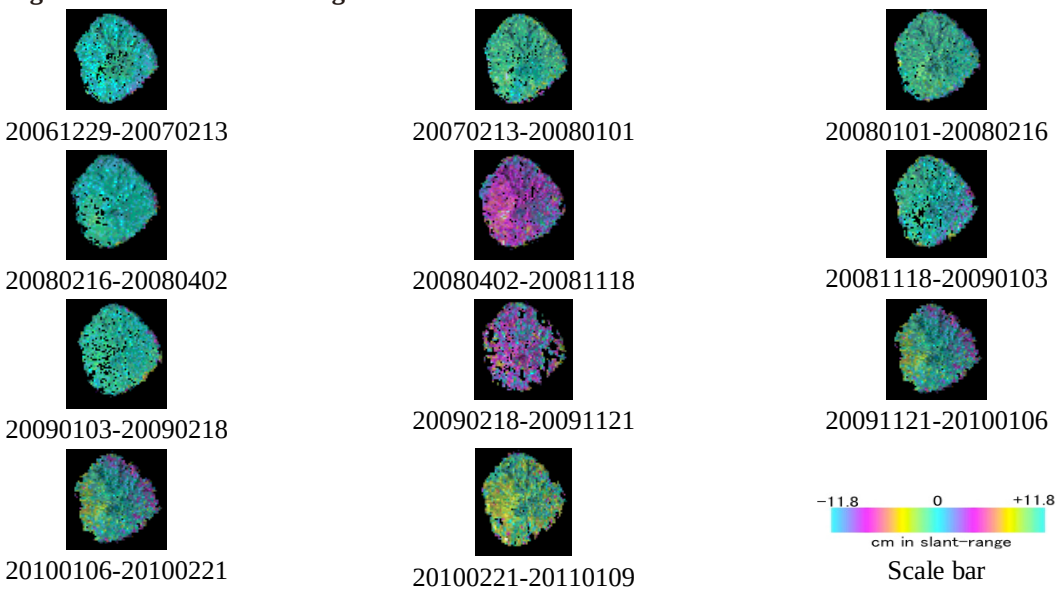

Figure 2. Interferogram results from ascending data.

Interferogram result from descending data

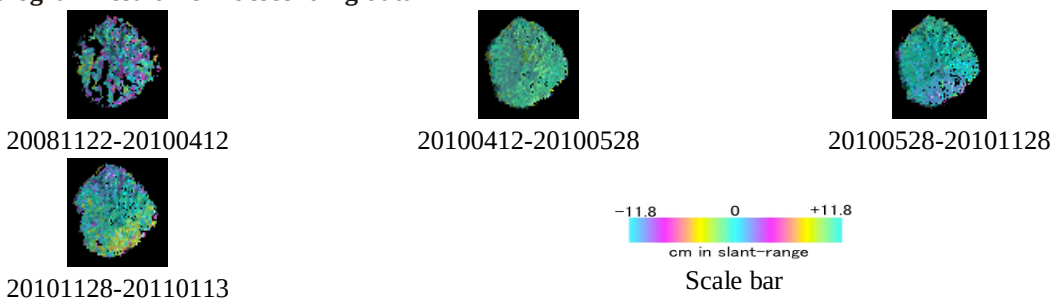

Figure 3. Interferogram results from ascending data.

Discussion

L-band interferograms are usually affected by ionosphere contribution. Therefore, it is essential to mitigate the effect to interpret the results correctly. Several approaches, for instances, range split-spectrum (Brcic et al., 2010), range phase group delay (Meyer et al., 2006), or multiple aperture interferometry and its along-track integration (Jung et al., 2013) have been proposed to mitigate the ionospheric contribution particularly in the L-band. Meanwhile, the ionospheric impact on SAR data is less in the higher frequency. In the C-band the effect is only about one-sixteenth of the L-band (Liang et al., 2019). We utilize polynomial order to mitigate long wavelength-trend induced by the ionosphere. Figure 4 is the effect of the ionosphere on pair 20100106_20100221 (for the whole interferogram on that pair) and the detrending result. Even though we can minimize the ionosphere contribution, the troposphere contribution still exists. We can see in Figure 4 phase jumps not following the long-wavelength trend appear. This phase jump is the water vapor contribution in the troposphere layer (R. Hanssen, 1998).

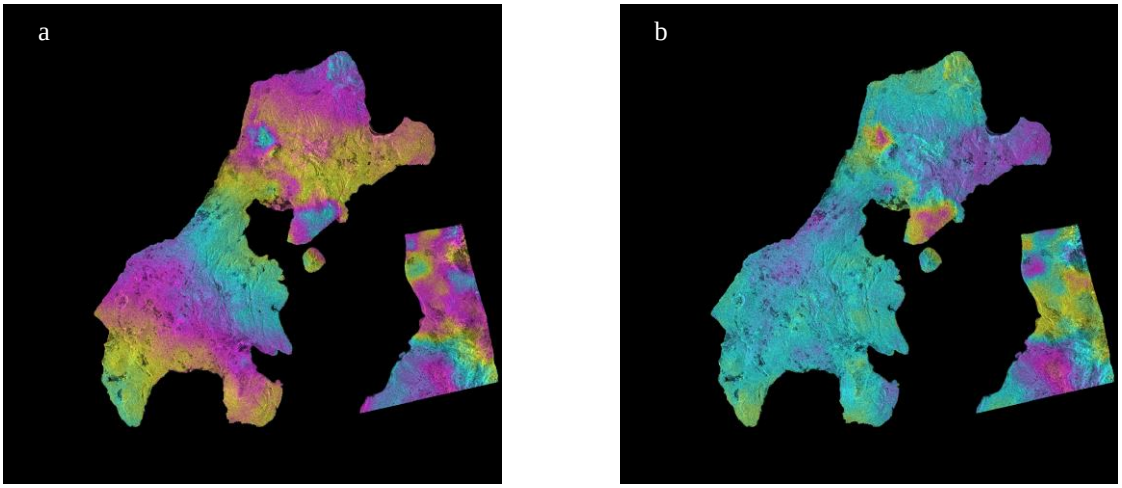

Figure 4. (a) The effect of ionosphere mimic long wavelength trend, and (b) detrending result.

As we observe, holes appear in unwrapping results for some ascending pairs (20080216-20080402, 20081118-20090103, and 20090218-20091121) and descending pairs (20081122-20100412, 20100528-20101128, and 20101128-20110113). These are due to lost coherence mainly because of noise and long temporal baseline. Thus, we have difficulties identifying deformation signals in these particular interferogram pairs.

Despite difficulties interpreting the result in lost coherence pairs, we observe episodic deformation signal in interferogram pair 20080402-20081118 (Figure 2). The deformation signal reaches 6.4 cm moving away from the satellite line of sight. We may follow the proposed mud volcano model developed by Barber et al., 1986 to describe the existence of deformation in the Kambing Island mud volcano. Moreover, observation from optical satellite imagery and cross-section profiles acquired from Google Earth can elucidate mud buildup near the mud volcano conduit (Figure 5). Nonetheless, we suggest the importance of field surveys and long-term InSAR methods, such as the Small BAseline Subset (Lanari et al., 2004), to support our findings.

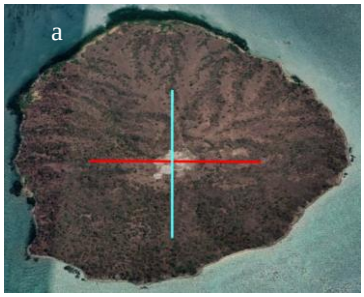

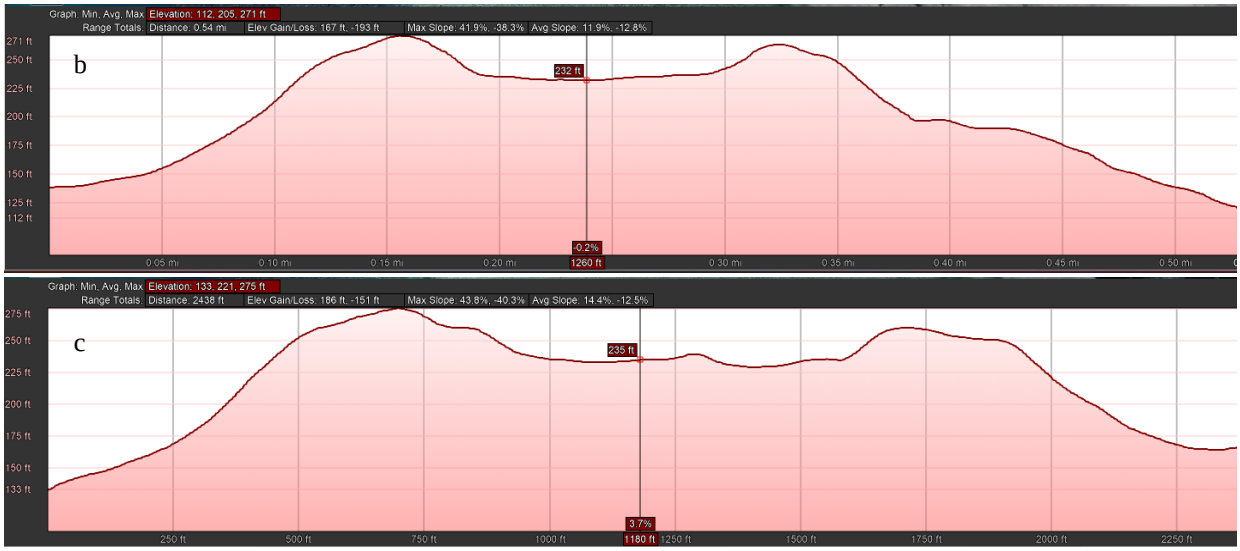

Figure 5. (a) Kambing Island observed using Google Earth, (b) Cross section from North to South (blue line), (c) Cross section from West to East (red line)

CONCLUSIONS

Using L-band InSAR, the mud volcano deformation in Kambing Island is difficult to identify due to lost coherence (in some pairs) and atmosphere (particularly troposphere layer) contribution. Nevertheless, we could locate episodic deformation reaches 6.4 cm moving away from the satellite line of sight in interferogram pair 20080402-20081118. Optical satellite observation indicates a buildup of mud layer from the mud volcano conduit, which agrees with our findings in L-band interferograms. However, direct observation and long-term InSAR are desired to support our results.

ACKNOWLEDGEMENTS

The ALOS/PALSAR data in this study are shared among PIXEL (PALSAR Interferometry Consortium to Study our Evolving Land Surface) under a cooperative research contract with the Earthquake Research Institute, University of Tokyo. The ownership of ALOS/PALSAR data belongs to the JAXA (Japan Aerospace Exploration Agency). Some of the figures are created using GMT software .

CONFLICT OF INTERESTS

The authors declare they do not have conflict of interest.

REFERENCES

Antonielli, B., Monserrat, O., Bonini, M., Righini, G., Sani, F., Luzi, G., Feyzullayev, A. A., & Aliyev, C. S. (2014). Pre-eruptive ground deformation of Azerbaijan mud volcanoes detected through satellite radar interferometry (DInSAR). *Tectonophysics*, *637*, 163–177. https://doi.org/10.1016/j.tecto.2014.10.005

Barber, A. J., Tjokrosapoetro, S., & Charlton, T. R. (1986). Mud Volcanoes, Shale Diapirs, Wrench Faults, and Melanges in Accretionary Complexes, Eastern Indonesia^ The importance of shale diapirism in the formation of. In *The American Association of Petroleum Geologists Bulletin V* (Vol. 70, Issue 11).

Brcic, R., Parizzi, A., Eineder, M., Bamler, R., & Meyer, F. (2010). Estimation and compensation of ionospheric delay for SAR interferometry. *International Geoscience and Remote Sensing Symposium (IGARSS)*, *3*, 2908–2911. https://doi.org/10.1109/IGARSS.2010.5652231

Costantini, M. (1998). A Novel Phase Unwrapping Method Based on Network Programming. In *IEEE TRANSACTIONS ON GEOSCIENCE AND REMOTE SENSING* (Vol. 36, Issue 3).

Dimitrov, L. I. (n.d.). *Mud volcanoes-the most important pathway for degassing deeply buried sediments*. www.elsevier.com/locate/earscirev

Fukushima, Y., Mori, J., Hashimoto, M., & Kano, Y. (2009). Subsidence associated with the LUSI mud eruption, East Java, investigated by SAR interferometry. *Marine and Petroleum Geology*, *26*(9), 1740–1750. https://doi.org/10.1016/j.marpetgeo.2009.02.001

Funning, G. J., & Garcia, A. (2019). A systematic study of earthquake detectability using Sentinel-1 InterferometricWide-Swath data. *Geophysical Journal International*, *216*(1), 332–349. https://doi.org/10.1093/gji/ggy426

Goldstein, R. M., & Werner, C. L. (1998). Radar interferogram filtering for geophysical applications. *Geophysical Research Letters*, *25*(21), 4035–4038. https://doi.org/10.1029/1998GL900033

Hanssen, R. (1998). *Atmospheric heterogeneities in ERS tandem SAR interferometry* (Issue 98). http://doris.tudelft.nl/Literature/hanssen98i.html

Hanssen, R. F. (2002). *Radar Interferometry, Data Interpretation and Error Analysis*.

Hussain, E., Wright, T. J., Walters, R. J., Bekaert, D., Hooper, A., & Houseman, G. A. (2016). Geodetic observations of postseismic creep in the decade after the 1999 Izmit earthquake, Turkey: Implications for a shallow slip deficit. *Journal of Geophysical Research: Solid Earth*, *121*(4), 2980–3001. https://doi.org/10.1002/2015JB012737

Iio, K., & Furuya, M. (2018). Surface deformation and source modeling of Ayaz-Akhtarma mud volcano, Azerbaijan, as detected by ALOS/ALOS-2 InSAR. *Progress in Earth and Planetary Science*, *5*(1). https://doi.org/10.1186/s40645-018-0220-7

Jung, H. S., Lee, D. T., Lu, Z., & Won, J. S. (2013). Ionospheric correction of SAR interferograms by multiple-aperture interferometry. *IEEE Transactions on Geoscience and Remote Sensing*, *51*(5), 3191–3199. https://doi.org/10.1109/TGRS.2012.2218660

Kopf, A. J. (2002). Significance of mud volcanism. *Reviews of Geophysics*, *40*(2), 2-1-2–52. https://doi.org/10.1029/2000RG000093

Liang, C., Agram, P., Simons, M., & Fielding, E. J. (2019). Ionospheric correction of InSAR time series analysis of C-band sentinel-1 TOPS data. *IEEE Transactions on Geoscience and Remote Sensing*, *57*(9), 6755–6773. https://doi.org/10.1109/TGRS.2019.2908494

Masato Furuya. (2011). *Sar Interferometry*. 1–24. https://doi.org/10.1007/978-90-481-8702-7

Meyer, F., Bamler, R., Jakowski, N., & Fritz, T. (2006). The potential of low-frequency SAR systems for mapping ionospheric TEC distributions. *IEEE Geoscience and Remote Sensing Letters*, *3*(4), 560–564. https://doi.org/10.1109/LGRS.2006.882148

Milkov, A. V. (n.d.). *Worldwide distribution of submarine mud volcanoes and associated gas hydrates*. www.elsevier.nl/locate/margeo

Moreira, A., Prats-iraola, P., Younis, M., Krieger, G., Hajnsek, I., & Papathanassiou, K. P. (2013). *A Tutorial on Synthetic Aperture Radar*. *march*.

Wessel, P., W. H. F. Smith, R. Scharroo, J. Luis, and F. Wobbe, Generic Mapping Tools: Improved Version Released, EOS Trans. AGU, 94(45), p. 409–410, 2013. doi:10.1002/2013EO450001.